# EXPERIMENTAL MODELING OF TSUNAMI GENERATED BY UNDERWATER LANDSLIDES

Langford P. Sue and Roger I. Nokes
Department of Civil Engineering, University of Canterbury
Christchurch, New Zealand

Roy A. Walters
National Institute for Water and Atmospheric Research
Christchurch, New Zealand

## ABSTRACT

Preliminary results from a set of laboratory experiments aimed at producing a high-quality dataset for modeling underwater landslide-induced tsunami are presented. A unique feature of these experiments is the use of a method to measure water surface profiles continuously in both space and time rather than at discrete points. Water levels are obtained using an optical technique based on laser induced fluorescence, which is shown to be comparable in accuracy and resolution to traditional electrical point wave gauges. The ability to capture the spatial variations of the water surface along with the temporal changes has proven to be a powerful tool with which to study the wave generation process.

In the experiments, the landslide density and initial submergence are varied and information of wave heights, lengths, propagation speeds, and shore run-up is measured. The experiments highlight the non-linear interaction between slider kinematics and initial submergence, and the wave field.

The ability to resolve water levels spatially and temporally allows wave potential energy time histories to be calculated. Conversion efficiencies range from 1.1%-5.9% for landslide potential energy into wave potential energy. Rates for conversion between landslide kinetic energy and wave potential energy range between 2.8% and 13.8%.

The wave trough initially generated above the rear end of the landslide propagates in both upstream and downstream directions. The upstream-travelling trough creates the large initial draw-down at the shore. A wave crest generated by the landslide as it decelerates at the bottom of the slope causes the maximum wave run-up height observed at the shore.

# 1. INTRODUCTION

Tsunami are a fascinating but potentially devastating natural phenomenon that have occurred regularly throughout history along New Zealand's shorelines, and around the world. With increasing populations and the construction of infrastructure in coastal zones, the effect of these large waves has become a major concern. There are several reasons tsunami are hazardous. Firstly it is their size, with waves several hundred metres in height known to have occurred in the past (Murty 2003; New Scientist 2004). The highest recorded wave run-up was generated in 1958 following a sub-aerial landslide in Lituya Bay, Alaska. This impulse wave caused deforestation and soil erosion down to bedrock level to an elevation of 524 m, and has been modeled experimentally by Fritz et al (2001). Secondly, tsunami can travel at considerable speeds, upwards of many hundreds of kilometres per hour. Lastly, tsunami occurrences are unpredictable. Seismic events such as earthquakes and landslides, the generation mechanisms of tsunami, occur sporadically in time and space, and not all seismic events have generated significant waves. Studies of historical records and forensic analysis of coastal geology have shown significant wave events occur frequently across the world. Many natural phenomena are capable of creating tsunamis. Of particular concern is the underwater landslide-induced tsunami, due to the potentially short warning before waves reach the shore. Sections of sediment or rock on the seabed can slide into deeper water, and this movement translates into a disturbance on the water surface above.

Experimental research into submarine landslide-induced tsunami began in 1955 to dispel the belief of many at the time that disturbances such as submarine landslides were unlikely to cause tsunami. The type of submarine mass failure is based on the landslide geometry and on the characteristics of the failure material, such as chemical composition, grain size, and density. Due to the inherent difficulties with scaling of these factors, the landslide failure mass is often approximated experimentally by a solid mass, either triangular or semi-elliptical in shape.

Wiegel (1955) preferred to experiment with sliding and falling blocks of various shapes, sizes, and densities, as opposed to granular slide experiments. These two-dimensional tests were performed in a constant depth channel, and factors such as initial submergence, slide angle, and water depth were varied, and the wave characteristics were measured using parallel-wire resistance wave gauges at both near and far field locations. Surface time histories of the tests downstream of the disturbance showed a crest formed first, followed by a trough with amplitude one to three times that of the first crest, and followed by a crest with a similar magnitude to the trough. It was found that dispersive waves were generated, as crests and troughs continued to be generated with increasing distance, and the amplitudes of the waves diminished as they propagated. The magnitude of the wave heights were found to depend primarily on the block weight, initial submergence, and water depth. The period of the waves was found to increase with increasing block length and decreasing incline angle. A dimensional analysis concluded that no parameters could be neglected. Instead, certain parameters were found to be related in such a way that it was not possible to hold all but one constant to determine their individual effects. Computations indicated approximately 1% of the initial net submerged potential energy of the sliding block was transferred into wave energy, with this percentage increasing with reduced initial submergence and decreasing water depth.

Other experimentalists have chosen to simulate a submarine landslide with a right-triangular prism sliding down a 45° slope (Rzadkiewicz et al. 1997; Watts 1997; Watts 1998; Watts 2000; Watts and Grilli 2003). The two-dimensional experiments of Rzadkiewicz et al. (1997) were a short series of tests to produce data to compare directly with some of their numerical models. These tests involved right-triangular simulated landslide masses, consisting of solid material, and granular sand and gravel, sliding down 30° and 45° slopes. Side-on images were captured at 0.4 s and 0.8 s after slide release, and from these landslide material shape and water level profiles were determined.

Watts' (1997) experiments were similar, consisting of solid and granular slides along a 45° slope. However, a wider parameter space was investigated, with slide material, initial submergence, porosity, and

density varied. Resistance wave gauges were used to measure water level time-histories at various locations downstream of the slide, and a micro-accelerometer recorded the landslide's centre-of-mass motion. A comparison of the motions of granular slide material with the motions of a solid block, by using a variety of granular materials to simulate the landslide failure mass, found that the centre of mass motion of a granular slide was similar to that of a solid block slider. This study also tried to develop a non-dimensional framework in which to predict maximum wave amplitudes (wave troughs) from specific landslide parameters such as landslide length and initial submergence.

Some of the later experimental research is in three-dimensional wave experiments with both angular, semi-hemispherical (Liu et al. 2005; Raichlen and Synolakis 2003), and streamlined solid block slider shapes (Enet et al. 2003). The large-scale tests of Raichlen and Synolakis (2003), attempting to minimise the effects of viscosity and capillary action, consisted of a 91 cm long, 46 cm high, and 61 cm wide triangular wedge-shaped block sliding down a planar (1 V:2 H) slope. The 475.52 kg block started its slide at various submergences from fully submerged to partially aerial. A micro-accelerometer and position indicator recorded the block location time-histories, and an array of resistance wave gauges recorded the propagating waves and run-up heights on the beach behind the sliding mass. The three-dimensional simulated submarine landslide tests of Enet et al. (2003) were developed to produce experimental data suitable for comparison with their numerical model results. The flattened dome-like slider block had a thickness of 80 mm, a length of 400 mm, a width of 700 mm, and a bulk density of 2,700 kg/m$^3$. The initial submergence was varied and its motions as it slid down the 15° slope were recorded with a micro-accelerometer located at the block's centre-of-mass. The propagating wave field generated was measured with an array of four capacitance wave gauges.

In an effort to produce comparable results from their numerical models, the international tsunami research community defined a benchmark configuration for studying the generation of tsunami by underwater landslides. This was deemed necessary due to the difficulties in interpreting the results from the various experimental and numerical models incorporating a wide range of constitutive behaviours (Grilli et al. 2003; Watts et al. 2001). It was also noted that the sharp edges of the triangular sliding blocks used in previous experimental studies were difficult to model computationally due to the strong flow separation at the vertices. Apart from reef platform failures, this shape was considered to be unrepresentative of the geometry of most underwater mass failures. The tsunami community's recommendation was for a smoother, more streamlined shape which, despite its idealisation, would represent the majority of real events (Grilli et al. 2003).

Two-dimensional tests were recommended as they presented fewer difficulties than three-dimensional tests for numerical modeling. The benchmark configuration consisted of a semi-elliptical block sliding down a planar slope at 15° from the horizontal. The landslide had a thickness:length ratio of 1:20 and a specific gravity of 1.85. It was completely submerged, with the centre of the top surface initially submerged 0.259 times the length of the landslide. A basic set of experiments with this arrangement was performed, but the quality of the results were inadequate to validate numerical models due to electrical point wave gauge accuracy (Watts et al. 2001).

The work of Fleming et al (2005) also experimented with this benchmark configuration. Sets of experiments were performed with a semi-elliptical block and water levels were recorded with three resistance wave gauges. The data generated was to be compared with the results of Watts et al (2001). Further experiments with triangular solid and granular slides were completed to examine the effects of initial landslide shape, initial submergence, volume, density, and deformability. Water levels in the near- and far-field were measured with an array of five wave gauges.

Experimental laboratory test results are generated using grossly simplified geometries and are inherently difficult to scale up to full-size. To model each tsunami scenario in the laboratory at sufficient scale and complexity to account for landslide deformations and ocean bathymetry would prove to be extremely costly. As such, laboratory experiments are used to observe specific features of tsunami generated

by sliding masses in a controlled manner, and numerical models take into account the various shoreline and deep-ocean geometries when used to predict full-sized events.

A variety of computational models have been developed by researchers to look at the many different phenomena associated with submarine landslides and tsunami. Each model makes certain assumptions in order to simplify the governing equations of fluid dynamics. These assumptions are associated with fluid viscosity, landslide friction, and wave linearity. There are models for slope failure (Martel 2004), landslide and water interaction (Jiang and Leblond 1992), wave generation and propagation (Enet et al. 2003; Grilli et al. 2002), and wave run-up (Kanoglu 2003; Kennedy et al. 2000; Liu et al. 2005; Synolakis 1987; Tarman and Kanoglu 2003; Walters 2003). Most models use a finite or boundary element approach (Grilli et al. 2002; Mariotti and Heinrich 1999; Rzadkiewicz et al. 1997).

The more complex models are able to predict fluid parameters such as water level, wave run-up, and sub-surface velocities and pressures, varying in three spatial dimensions and over time. There are also several simple methods for predicting gross wave properties, such as maximum expected wave heights. Murty (2003) used information available in the literature to find a simple empirical linear relationship between landslide volume and the maximum observed wave heights. Another simplified model, used to couple the landslide mass to the generated waves, was to determine the amount of energy transferred from the block's initial gravitational potential energy to the potential energy of the waves. This is found to be of the order of 1% - 2% (Jiang and Leblond 1992; Ruff 2003; Tinti and Bortolucci 2000; Watts 1997).

Wave run-up at planar beaches has been studied in significant detail in the past (Kanoglu 2003; Kennedy et al. 2000; Liu et al. 2005; Synolakis 1987; Tarman and Kanoglu 2003; Walters 2003). These models studied run-up from waves generated from distant sources and looked at their transformation, breaking, and run-up as they approached the shore. In an underwater landslide, the failure mass motion will be away from shore, generating waves that also move offshore. However, little work has looked at the wave run-up at the beach behind the landslide, as it is this that is of immediate danger to the population and infrastructure in the proximity of the slide.

Individual models are tested using different geometries and motions, which make comparisons between models difficult (Grilli et al. 2002; Grilli and Watts 1999; Mariotti and Heinrich 1999; Rzadkiewicz et al. 1997). Also, many of these models have been developed in isolation from submarine landslide geomorphology, and are therefore difficult to apply to real situations. Even when there are large amounts of field data available to validate these models, such as from the 1998 Papua New Guinea event, there are difficulties and controversies plaguing their interpretation (Davies et al. 2003; Imamura and Hashi 2003; Lynett et al. 2003; Okal 2003; Satake and Tanioka 2003; Tappin et al. 2003; Tappin et al. 2001). Experimental tests are a means to validate these numerical models. To some extent validated models possess some predictive qualities.

The following sections contain information pertaining to the laboratory experiments conducted at the University of Canterbury. Details of the experimental set-up are given in Section 2, along with information on the methods developed to measure the wave phenomena. Some preliminary results are given and discussed in Section 3, followed by some concluding remarks in Section 4. Further details regarding the experimental methods can be found in Sue et al (2006). Additional results from the experimental tests will be included in future papers, with full results and numerical model comparisons to be included in Sue (in preparation).

## 2. METHODS

The motivation behind this experimental programme was to generate a comprehensive dataset using the benchmark configuration defined by the international tsunami research community (Grilli et al. 2003; Watts et al. 2001). The data from this study would be of sufficient quality for comparisons with numerical models. The same two-dimensional configuration as Watts et al (2001) was used. This consisted of a model landslide with a thickness:length ratio of 1:20. However, unlike their experiments, a variety of landslide densities and initial submergences were investigated here.

The following sections describe the experimental programme and set-up. This is followed by information on the Particle Tracking Velocimetry (PTV) technique used to measure the landslide kinematics. The development of the Laser Induced Fluorescence (LIF) technique, to measure the water levels, is also presented along with details of its capabilities compared with traditional electrical wave gauges.

### 2.1 EXPERIMENTAL PROGRAMME

An experimental programme was completed to measure the landslide motions and wave fields generated by laboratory underwater landslides with fifteen combinations of specific gravity and initial submergence. Specific gravity is defined as the ratio of the total unsubmerged mass of the block, $m_b$, and the mass of water displaced by the landslide, $m_o$, as shown in Equation 1.

$$\text{specific gravity} = m_b / m_o \tag{1}$$

Equation 2 defines the non-dimensional initial submergence as the ratio of the depth of water directly above the landslide centre of mass at its initial starting position, d, and the length of the landslide block along the slope, b. A diagram of the experimental set-up is included in Figure 1.

$$\text{initial submergence} = d / b \tag{2}$$

The testing programme consisted of a model landslide block with a combination of five different specific gravities and five initial submergences, as presented in Table 1. Test SG5-IS5 combined the highest specific gravity with the shallowest initial submergence, and produced the largest water level response. SG5-IS1 combined the heaviest specific gravity with the deepest submergence, while SG1-IS5 combined the lightest specific gravity with the shallowest submergence, and both of these produced some of the smallest responses. A range of combinations was not tested as they were expected to create small waves and suffer from resolution issues. The repeatability of the experimental techniques were rigorously assessed, details of which have not been included here, but appear in Sue et al (2006). Test repeatability was important because it allowed different testing methods to be used sequentially, instead of simultaneously, resulting in reduced experimental complexity.

**Table 1. Experimental test combinations of Specific Gravity (SG) and Initial Submergence (IS).**

| | | | | | | | |
|---|---|---|---|---|---|---|---|
| **Specific Gravity:** | | | | | | | |
| | 5 variations | | Lightest | **SG1** | 1.63 | | |
| | | | | **SG2** | 2.23 | | |
| | | | | **SG3** | 2.83 | | |
| | | | | **SG4** | 3.42 | | |
| | | | Heaviest | **SG5** | 4.02 | | |
| | | | | SG = Specific Gravity | | | |
| **Initial Submergence:** | | | | | | | |
| | 5 variations | | Deepest | **IS1** | 0.5 | d/b | |
| | | | | **IS2** | 0.4 | d/b | |
| | | | | **IS3** | 0.3 | d/b | |
| | | | | **IS4** | 0.2 | d/b | |
| | | | Shallowest | **IS5** | 0.1 | d/b | |
| | | | | IS = Initial Submergence | | | |
| | | | | d = depth of water above landslide CoM | | | |
| | | | | b = block length (500mm) | | | |
| **Combinations tested:** | | | | | | | |

| | IS5 | IS4 | IS3 | IS2 | IS1 |
|---|---|---|---|---|---|
| **SG5** | * | * | * | * | * |
| **SG4** | * | * | * | * | |
| **SG3** | * | * | * | | |
| **SG2** | * | * | | | |
| **SG1** | * | | | | |

## 2.2 EXPERIMENTAL SET-UP

The wave tank used in these experiments was a 0.250 m wide, 0.505 m deep, and 14.7 m long flume in the University of Canterbury's Fluid Mechanics Laboratory. The tank was filled with tap water to a depth of 435 mm. This flume was housed in a room with all windows and other openings blacked out to reduce outside light interference and to contain the laser light when it was operating in the darkened room.

An inclined ramp at an angle of 15° to the horizontal was placed at one end of the flume, and strips of stainless steel and PVC sheeting were imbedded into the surface of the slope. The mildly flexible stainless steel strips were used to provide a means for the surface of the slope to transition smoothly from the 15° slope to the horizontal floor of the flume, and allow the landslide to slide down the slope and then along the floor where it would eventually stop due to friction. Profiles of the curved steel strips were cut from acrylic and fixed underneath to provide rigid support. The PVC strips were used to provide a more slippery surface upon which the landslide would slide compared to the acrylic and stainless steel base material, and could be easily replaced when worn.

The prismatic semi-elliptical model landslide was milled from a solid block of aluminium. The block length, b, was 0.5 m (major axis length) and was 0.026 m thick (minor axis = 0.052 m), and 0.25 m wide. The total volume of the block was 2.419 litres. Hollow cavities were incorporated into the base of the block that could be filled with polystyrene or lead shot ballast to vary the total specific gravity of the landslide. A plastic sheet was screwed into place to cover the cavities and secure the ballast. To minimise the reflectivity, the landslide block was painted matt black. A photograph of the aluminium slider block is included in Figure 1. To further minimise the sliding friction, 3 mm diameter hardened steel balls were embedded into the base of the block, at the four corners along the leading and trailing edges. To lubricate the steel balls and PVC strips, silicone grease was applied to the slope surface. A length of fishing line, attached to the trailing edge of the block, was used to anchor the block to the release mechanism and hold it at the correct initial submergence prior to each experimental run. Different submergences were achieved by using different lengths of fishing line.

Initial investigations showed that the wave field generated was highly dependent on the stopping mechanism, and previous experimentalists failed to note what technique they used to stop their sliding blocks when they reached the bottom of the slope. It is assumed that the blocks just topple over and stop when they reach the end of the slope, and their wave records end before this time. For heavier blocks with high accelerations and velocities, these times can be quite short. This does not allow sufficient time to observe the waves as they develop and propagate. To see the effect abruptly stopping the block at the toe of the slope had on the wave field, a tether was attached to the landslide that was just long enough for the block to slide normally from its initial position until the end of the slope. It was found that a block coming to a sudden stop created waves larger than the waves that were generated by the landslide if it were sliding and decelerating naturally. It was considered desirable that the landslide be allowed to progressively transition from sliding down the slope to run out on the flume floor of its own accord. This minimised the waves being generated by the sudden stopping of the block, and was considered to more closely represent the deposition of actual underwater landslide masses sliding along shallow slopes.

## 2.3 EXPERIMENTAL TECHNIQUES

In this experimental programme, PTV was used to measure the motions of the landslide block as it slid down the slope. The PTV software used in this experimental program was FluidStream (Nokes 2005a), developed at the University of Canterbury for flow visualisation. White plastic sheeting was placed behind the flume to provide a white background. Fluorescent tube lights in the room and a halogen spotlight were used to illuminate the landslide. A series of red dots were applied to the side of the black coloured model landslide and a Canon MV30i colour digital video camera recorded the block's motion against the white background. Image sequences were captured and recorded to a computer using Adobe Premiere software. Image processing software was used to isolate the red dots from the black and white background of the white plastic sheeting and the black landslide. The PTV software was then used to track the red dot at the landslide centre of mass through the image sequence. The entire slope was too large to capture with adequate resolution from one camera placement so several camera positions were used and the landslide positions from each location were combined.

The use of electrical point wave gauges at specific locations can only give limited insights into the wave generation process, as the spatial changes in water profile between the gauge positions are not measured. There are also questions as to the influence of surface tension and meniscus effects on the gauge wires at the small laboratory scales, as well as the effect of having objects physically in the flow. To remedy this, a non-intrusive water level measurement technique was developed that minimised the disturbance to the water, and also captured the spatial as well as the temporal variations.

Recording water levels optically has many advantages over stationary point wave gauges, the main one being its ability to capture the spatial variation of the waves as well as the temporal variations. To avoid the menisci problems associated with recording the water levels at the sidewalls under ambient light conditions, a LIF technique was developed to capture the wave profiles and wave run-up heights away from the sidewalls. A small concentration of rhodamine 6G fluorescent dye was stirred into the flume water, and illuminated with a 1.0 W vertical laser light sheet orientated parallel with the longitudinal axis of the wave tank. The 0.1 mg/L dye concentration in the water column fluoresced due to excitation by the laser light, and this contrasted with the surrounding darkness of the blackened room. A high-resolution digital video camera was used to record a series of images of the illuminated water. In each frame the interface between the regions of high and low light intensity marked the location of the free surface. A diagram of the experimental set-up is shown in Figure 1. The camera used to capture images of the free surface response to the release of the model landslide was a Pulnix TM1010 monochromatic progressive scan camera with a 1008 x 1008 pixel resolution. An orange-colour filter was used to filter out the laser light from the fluorescent light. Image sequences were recorded at 15 Hz and were archived to computer hard disc as a series of JPEG images. To eliminate the interference of the water line at the sidewall nearest the camera, the

camera was mounted slightly higher than the water level to capture the water surface in the illuminated plane. This was taken into account in the analysis of the recorded images.

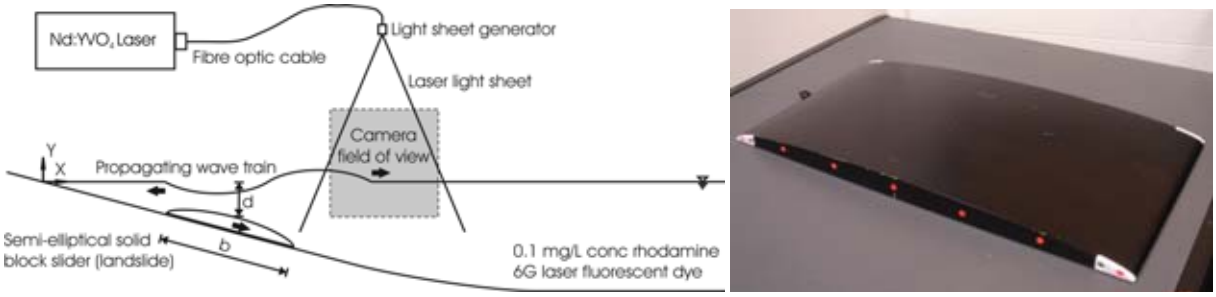


**Figure 1. Experimental set-up for LIF water level recording of submarine landslide-induced tsunami, and a photograph of the model landslide.**

ImageStream (Nokes 2005b), an image processing software package developed at the University of Canterbury, was used to determine the light intensity of each pixel in each of the JPEG images. The transition from the high intensity light of the fluorescing water to the low light intensity of the air signalled the location of the water surface. Sub-pixel resolution was achieved through a simple intensity interpolation process. The water levels were corrected for refraction and parallax errors, and a simple scaling procedure then transformed the water level from pixel space to physical space. Further details of the LIF technique and the analysis process are presented in Sue et al (2006).

To observe a substantial length of water surface with adequate resolution, the single camera was used to observe the flow in different locations for repeated runs of the same experiment. The camera and laser sheet were placed at the shoreline to record the propagation of the landslide-generated waves up the slope. The camera and light sheet were then moved further downstream to observe the downstream propagation and continued evolution of the waves. The water profiles were then combined to create a wide field of view of the surface response. The water surface profile experiments used 31 consecutive camera positions to record water levels from approximately 0.3 m upstream of the original shoreline to 10.1 m downstream.

To compare the performance of the LIF technique with traditional wave gauge methods, several tests were performed with both the LIF and point wave gauges operating simultaneously. Three Churchill Controls resistance wave gauges (RWG) were placed parallel to the laser sheet in the region above the base of the slope, approximately 0.145 m apart. The gauges were placed behind the light sheet so that they did not obscure the fluorescing water surface from the camera. Point LIF water level readings were determined at the same positions as the resistance wave gauges, and the two records compared. Tests in which large, moderate and very small waves were created were used to compare the two techniques. As illustrated in Figure 2, the LIF method produced point measurements of water level comparable to those of the RWGs. Note that each horizontal gridline represents two pixels in the plot of the largest waves, and one pixel in the small wave height plot.

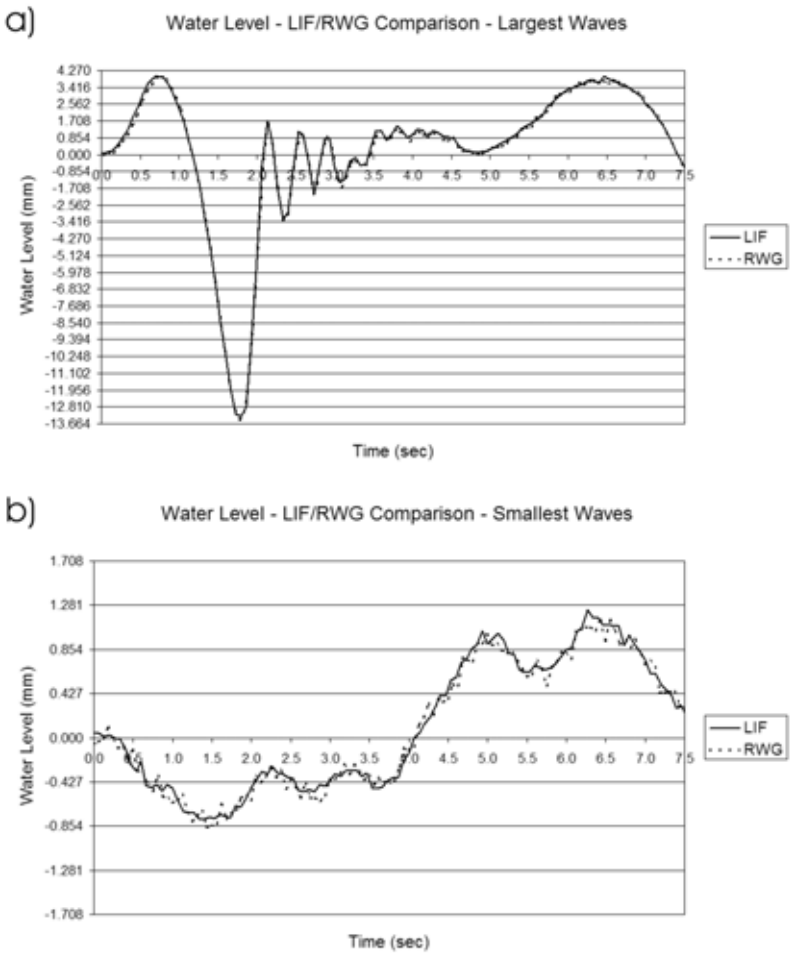


**Figure 2. Plots of LIF and RWG for comparison of performance for large and small wave heights. Note the different gridline intervals, as one pixel = 0.427 mm.**

## 3. EXPERIMENTAL RESULTS AND DISCUSSION

This section presents preliminary results from the experimental programme. It begins with details of the landslide kinematics, such as maximum landslide velocity and initial acceleration. Results from the water level measurements of wave amplitudes and run-up/down are then discussed. The percentage conversion of landslide potential energy into other forms of energy concludes this section. Some of the data presented in this section has been non-dimensionalised. Lengths such as water levels, run-up heights, and downstream positions have been non-dimensionalised by the landslide length, b. Accelerations have been non-dimensionalised by the gravitational acceleration, g, and times by $\sqrt{(g/b)}$.

### 3.1 LANDSLIDE KINEMATICS

An example of the landslide centre of mass velocity time history is shown in Figure 3 for the SG3_IS5 combination. The landslide velocity increases almost linearly from rest and reaches a maximum at the bottom of the slope, at which point the block slows and comes to rest along the flume floor. As indicated

by the increasing velocity of the landslide at the toe of the slope, terminal velocity is not reached. Velocity time histories for other combinations exhibited similar behaviour. This can be contrasted with the slider motions of Watts (1997), in which his landslides rapidly reached terminal velocity. Figure 3 also shows a time history plot of the landslide centre of mass acceleration for the SG3_IS5 test. The form of the acceleration plot is similar for all the specific gravity and initial submergence combinations, with only the magnitude and timing of the accelerations differing. The rapid increase to the peak acceleration typically occurs within two camera frames, or 0.133 seconds. Initial acceleration is taken as this peak value. The acceleration decreases slightly as the landslide progresses down the slope, before a rapid deceleration as the block reaches the base of the slope and transitions to sliding along the flume floor. A phase of roughly constant deceleration occurs as the landslide slows and finally stops. During the landslide experiments of Watts (1997), the accelerations peaked almost instantaneously before rapidly decreasing as the block approached terminal velocity. His acceleration time histories were typically measured for durations of 0.6 seconds.

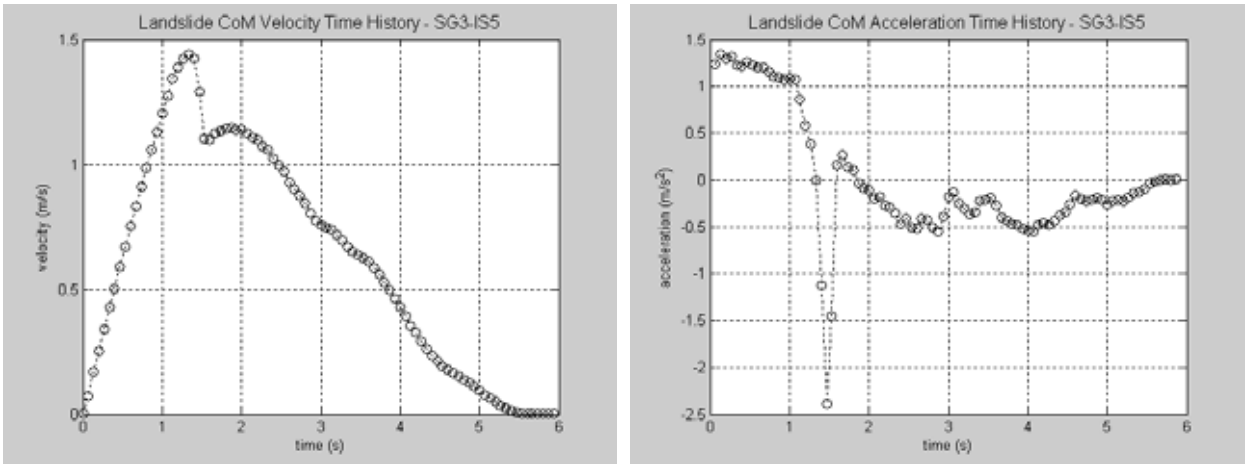


**Figure 3. Landslide centre of mass velocity and acceleration time histories for SG3_IS5 test.**

## 3.2 WAVE FIELDS

The evolution of the waves through space and time can be observed by looking at the water surface profiles. The changes in the lengths and total number of waves can be inspected. Figure 4 shows the water surface profiles of the SG3_IS5 test at successive times between 0.600 s and 5.600 s. Present in the first frame at time = 0.600 s is the 1st crest, 1st trough, and the beginnings of the 2nd crest, propagating downstream. The solid black bars indicate the approximate position of the landslide. The wave trough causing the run-down observed at the beach is also present as a trough propagating upstream. The following frames illustrate the evolution of these waves as they propagate. The 1st crest amplitude continues to increase initially, peaks, and then gradually decreases as the wave enters deeper water and its wavelength increases. The 1st trough and 2nd crest also exhibit this behaviour, although at later times. The continual generation of small amplitude waves with short wavelengths at the upstream end creates a propagating wave packet.

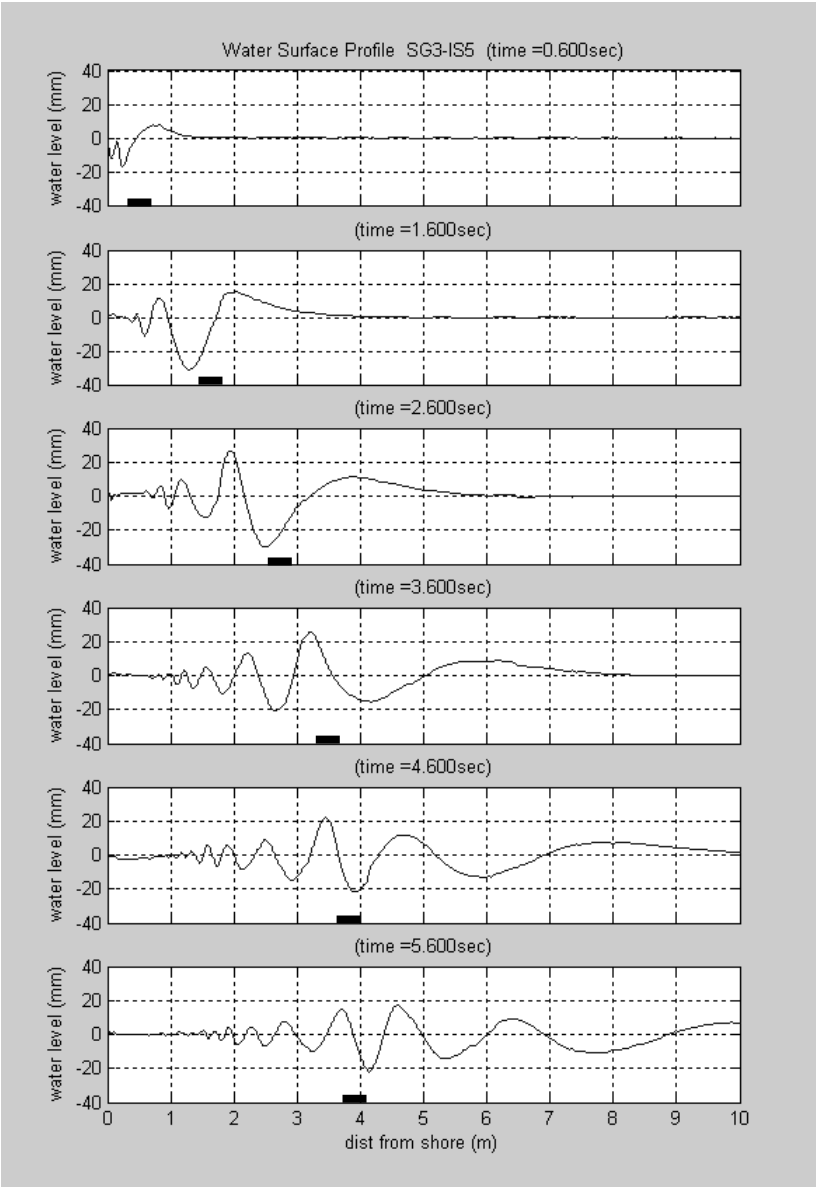


**Figure 4. Water surface profiles at time = 0.600, 1.600, 2.600, 3.600, 4.600, and 5.600 seconds for SG3_IS5 test. The solid black bars indicate the approximate position of the landslide.**

The water level profiles in Figures 4 are presented in a continuous manner in Figure 5. The plot in this figure displays water level, on the vertical axis, against time and downstream position on the horizontal axes. The red colours indicate positive water levels, or wave crests, and blue represents the negative water levels of troughs. The partially obscured black line indicates the downstream position of the landslide centre of mass. The evolution of the waves and the generation of the wave train are clearly illustrated. Figure 6 plots the three-dimensional water level data on a two-dimensional contour plot. In this form the wave propagation speeds are more clearly seen. The wave speeds relative to the landslide are also illustrated. From this plot it can be seen that the 1$^{st}$ crest forms ahead of the landslide centre of mass and the 1$^{st}$ trough forms behind it. The point at which these two waveforms meet follows the landslide centre of mass as it slides down the slope.

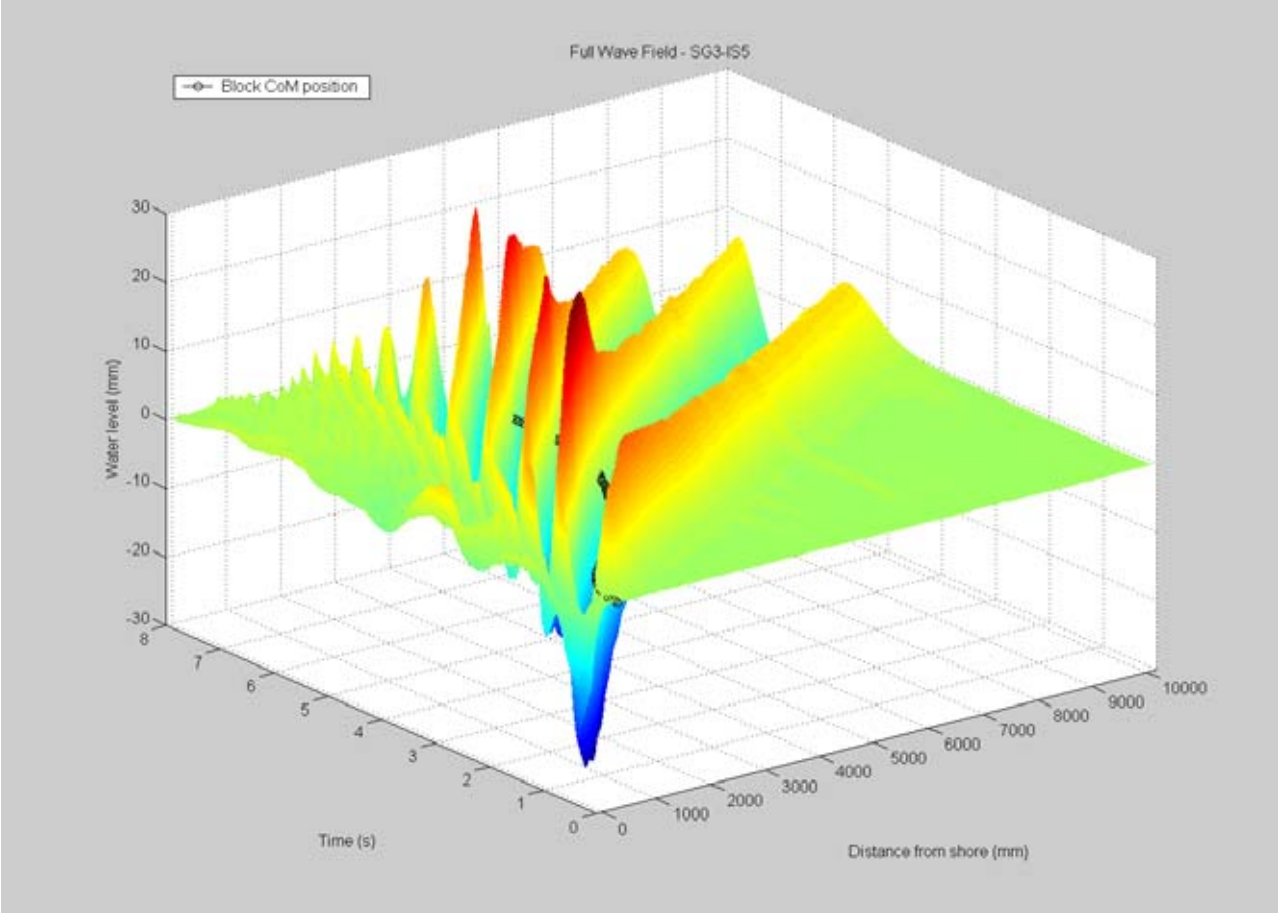


**Figure 5. Oblique three-dimensional views of water surface profile time history for the SG3-IS5 test.**

At this point, a qualitative description of the wave generation processes illustrated in two-dimensional contour plots of all fifteen combinations is given. The motion of the landslide generates the 1st crest as it pushes up the water ahead of it. The acceleration of the surrounding fluid creates a water pressure distribution over the moving landslide. The high pressures ahead of the landslide forces up the water surface above it to form the 1st wave crest. This crest is not attached to the landslide and propagates freely once generated. The accelerating fluid and the turbulent wake above and behind the sliding block creates a region of low pressure. This low pressure pulls the water surface down to form a depression. This wave trough is forced to propagate at the same speed as the accelerating landslide due to the low pressure region being directly connected to the sliding block. The 1$^{st}$ trough is free to propagate once the landslide reaches the bottom of the slope and begins to slow. The decrease in velocity of the block disrupts the low pressure region, and its connection with the trough can not be maintained.

Dispersion effects are also present, noticeable as the progressively slower speeds of waves further back in the wave train. The continual generation of waves at the trailing end of the train is also visible. The region of generation of these waves moves downstream over time. As individual waves are generated, their speeds increase as they move into deeper water. Also noticeable is the weak signal of disturbances propagating upstream of the slider, especially early in the wave generation process. These waves ultimately form the run-up and run-down observed at the shore.

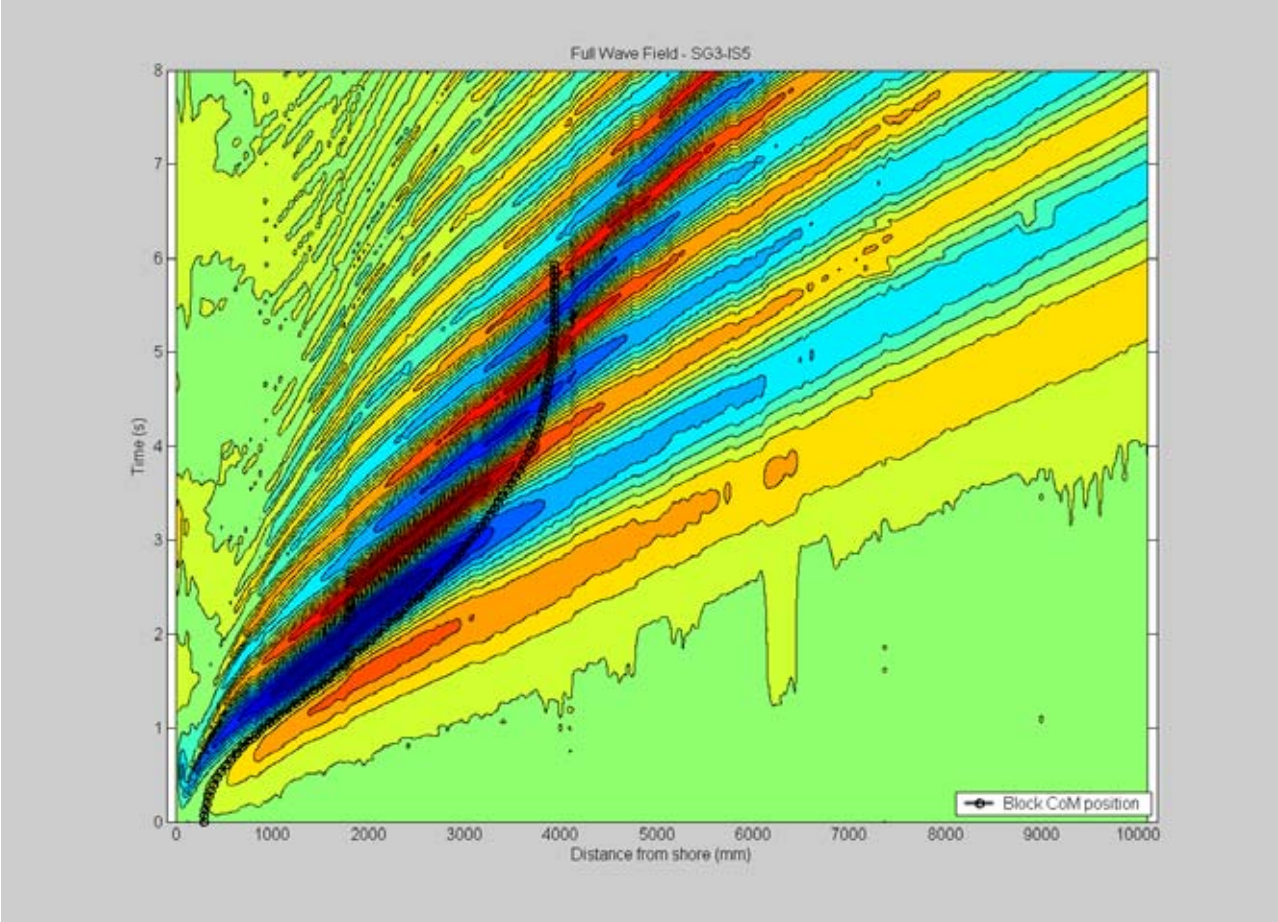


**Figure 6. Two-dimensional contour plot of water surface profile time history for the SG3-IS5 test. Red colours indicate wave crests and blue colours indicate wave troughs. Note the various wave speeds present within the wave train.**

The overall maximum crest amplitude and overall maximum trough amplitude for the fifteen test combinations are presented in Figure 7. These plots illustrate the increase in maximum crest and trough amplitude with heavier specific gravities and shallower initial submergences.

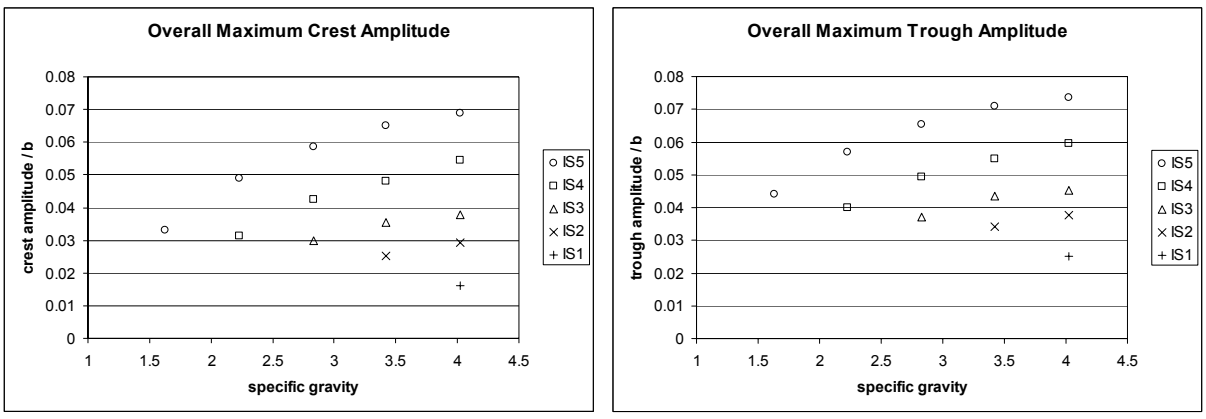


**Figure 7. Overall maximum crest amplitude and overall maximum trough amplitude as a function of specific gravity.**

The extent of wave run-up and run-down at the shore are also important parameters, as it is the wave magnitudes at the shore that are of immediate concern in practical situations. Indications of the likely draw-down and wave inundation, as well as the times at which these occur, are useful for communities with assets situated in the coastal area. Wave run-up and run-down heights along the slope were measured vertically from the original still water level. A typical wave run-up/down height time history is presented in Figure 8 for test SG3_IS5. The key features of this time history, and of those for other specific gravity and initial submergence combinations, is the large initial draw-down followed by a rebound to a level close to the original water level. This is followed by a positive run-up and relaxation back to the original mean water level.

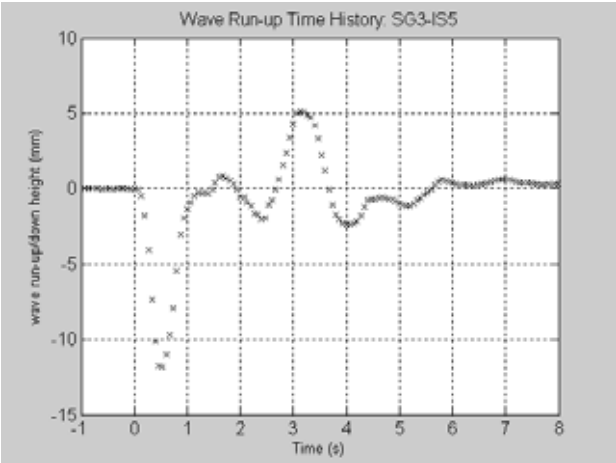


**Figure 8. Wave run-up/down height time history for the SG3_IS5 test.**

The trends observed in the maximum non-dimensional wave run-up data presented in Figure 9 indicate that the maximum wave run-up heights increase for heavier specific gravities and shallower initial submergences. We suggest that the positive run-up peak occurs as a result of a wave generated by the short duration, but high magnitude, deceleration of the landslide upon reaching the base of the slope. The wave generated at this point and time propagates upstream and runs up the slope. To provide further evidence of the landslide deceleration origins of the run-up height observed, Figure 9 also plots maximum non-dimensional wave run-up heights against maximum non-dimensional landslide decelerations at the base of the slope. The data from all fifteen combinations collapses onto one curve when the maximum deceleration is used as the independent variable.

Preliminary tests with the landslide block tethered so that it abruptly stopped at the base of the slope, resulted in the generation of waves with amplitudes larger than those initially generated by the accelerating landslide. The removal of the tether and allowing the landslide to slow naturally along the flume floor resulted in a significant reduction in the magnitude of the wave generated by the slowing block. However, the maximum positive run-up height was still dominated by the run-up of this landslide deceleration-induced wave. This indicates that landslide deceleration can have a significant affect on the magnitudes of the observed wave run-up.

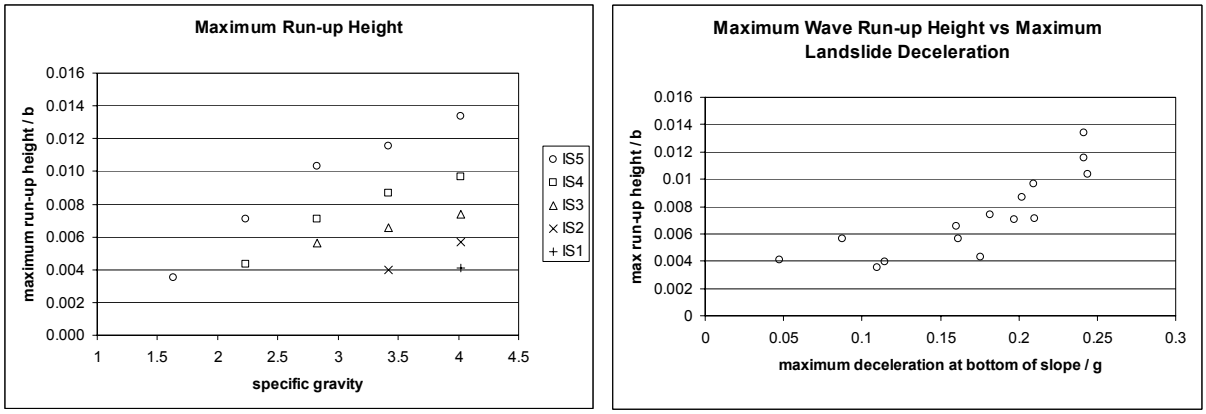


**Figure 9. Maximum wave run-up height as functions of specific gravity and maximum deceleration of the landslide at the base of the slope.**

Figure 10 indicates that the non-dimensional time of maximum run-up occurs earlier for higher specific gravities and deeper initial submergences. The added mass and shorter slope distances cause the landslide to reach the base of the slope earlier. As the run-up peak is most likely created by the deceleration of the block at toe of the slope, the maximum run-up occurs earlier. Based on this theory, the travel time for a wave generated above the toe of the slope to travel back to the beach was calculated. A wavelength of 0.5 m, equal to the length of the landslide, was assumed and the time for this wave to propagate upstream to the shore was added to the time for the landslide to reach the base of the slope. The ratio of the measured times to the calculated times of maximum run-up for all fifteen test combinations are very close to unity, and are plotted in Figure 10.

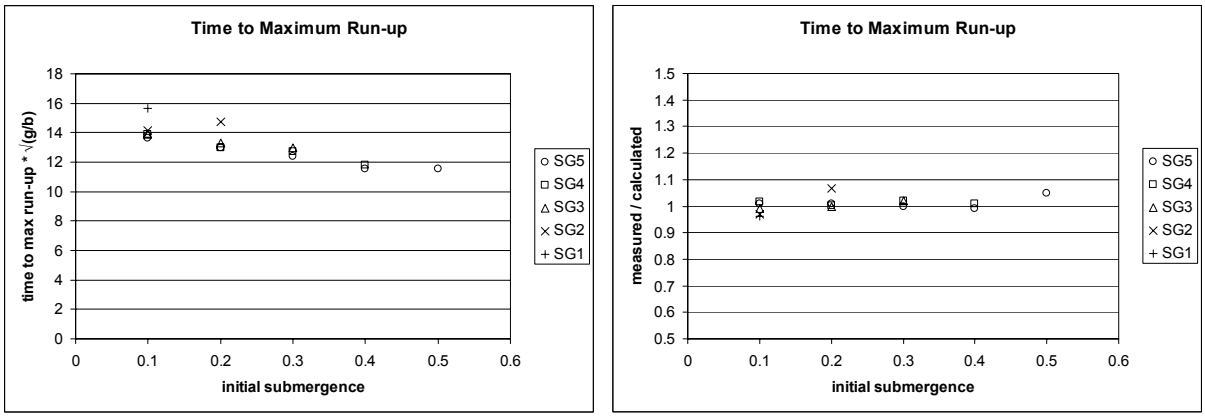


**Figure 10. Time of occurrence of maximum wave run-up height and a comparison of measured and calculated values, assuming a 0.5m wavelength crest was generated above the toe of the slope and propagated upstream, as a function of initial submergence.**

The magnitude of the non-dimensional wave run-down observed at the shore decreases with lighter specific gravities and deeper initial submergences, as shown in Figure 11. The wave run-down and the 1st wave trough are formed by the same mechanism, namely the initial draw-down of the water surface above the landslide. The depression that forms over the rear end of the block propagates in both the upstream direction, to cause the large initial draw-down at the shoreline, and downstream as the 1st wave trough. The magnitudes of these two parameters are governed by the strength of this initial water surface depression.

The correlation between the maximum run-down height and the maximum 1st wave trough amplitude, as shown in Figure 11, tends to confirm the common origin of these two phenomena.

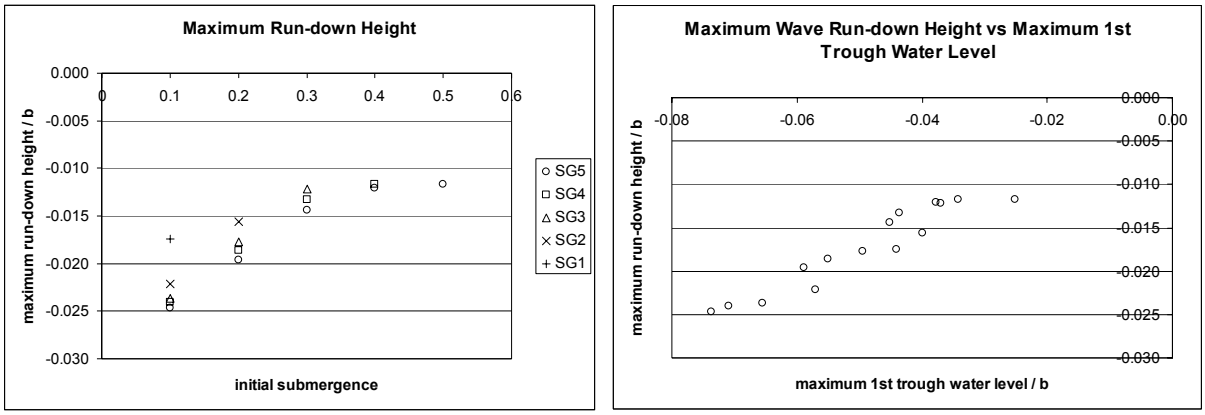


**Figure 11. Maximum wave run-down height as functions of specific gravity and maximum 1st trough amplitude.**

As shown in Figure 12, the non-dimensional time the maximum wave run-down occurs is independent of specific gravity, dependent solely on the initial submergence of the landslide. The maximum run-down occurs later for deeper submergences because the landslide is initially further downstream, and the initial water surface depression that forms over the landslide has further to travel upstream. An approximate time of occurrence of maximum wave run-down was calculated and compared with the measured values. Wave troughs with lengths of 0.4m, 0.5m and 0.6m, approximately the length of the landslide, were hypothetically generated at various downstream positions and propagated upstream towards the shore. These propagation times for the three different wavelengths are plotted in Figure 12 as a function of initial submergence. The correlation between the measured and calculated times is very good.

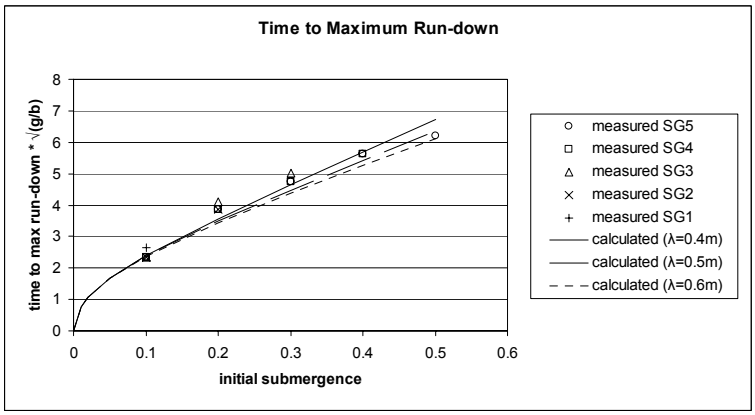


**Figure 12. Comparison of measured time of occurrence of maximum wave run-down with calculated values assuming a specific wavelength trough was generated above the initial landslide position and propagated upstream.**

## 3.3 ENERGY

Seismologists use the energy released during an earthquake to quantify the magnitude of the event. Similarly, wave potential energy, landslide potential energy, and landslide kinetic energy are possible measures as to an underwater landslide's potential for destruction. The time histories of the various energy forms also provide insights into the mechanisms in which the energy is transferred from the landslide

potential energy into other forms of energy, such as the wave field. This research appears to be the first experimental tsunami study in which full water surface profile time histories have been generated. The wave potential energy can be determined from this spatial and temporal water level information. Unfortunately it is not practicable to measure the internal kinetic energy of the water motions. The instantaneous potential energy contained in the waves was calculated with equation 3.

$$\text{wave } E_p(t) = \frac{1}{2}\rho_o g w \int_0^\infty \eta(t)^2 dx \tag{3}$$

In this expression for wave potential energy, $\rho_o$ is the density of water, $g$ is the acceleration of gravity, $w$ is the width of the flume and landslide, $\eta(t)$ is the water level as a function of time, $t$, and $x$ is the downstream position. The wave potential energy integration limits were actually between zero and 10.1 m downstream. However, provided waves had not propagated out of our observed domain and the water surface beyond 10.1 m was still, the integration of $\eta^2$ between zero and infinity was still valid. The instantaneous landslide kinetic energy was calculated as

$$\text{block } E_k(t) = \frac{1}{2} m_b vel(t)^2 \tag{4}$$

where $m_b$ is the unsubmerged landslide mass and $vel(t)$ is the instantaneous landslide velocity. The instantaneous landslide potential energy is calculated by multiplying the submerged mass of the landslide by the vertical fall distance relative to its initial position, and was calculated as

$$\text{block } E_p(t) = (m_b - m_0)(y(t_0) - y(t)) \tag{5}$$

where $m_o$ is the mass of water displaced by the landslide, $y(t_0)$ and $y(t)$ are the initial and instantaneous vertical position of the landslide respectively.

Figure 13 plots the time histories of wave potential energy, landslide kinetic energy, and the change in landslide potential energy, for the SG3_IS5 test. The key features of this plot are similar for the other combinations of specific gravity and initial submergence. Some of the block potential energy is converted into kinetic energy of the block as it slides down the slope. The remaining potential energy is dissipated as friction on the sliding surface. The motion of the landslide sets in motion some of the surrounding fluid, converting some of the block kinetic energy into kinetic energy of the water. Some of the energy in the water motions is then passed into the wave potential energy, the remainder being dissipated through friction. Note that wave potential energy decreases after approximately 4 seconds due to the propagation of energy out of the observed region. The maximum landslide kinetic energy occurs before the time of maximum landslide potential energy conversion because the block has started to slow before reaching the floor of the flume.

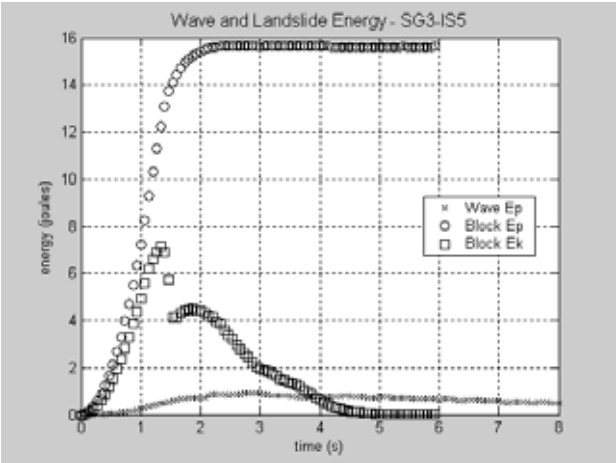


**Figure 13. Time histories of wave potential energy (wave Ep), landslide kinetic energy (block Ek), and landslide potential energy converted (block Ep), for the SG3_IS5 test.**

The values presented in Figure 14 indicate the maximum conversion of landslide kinetic energy into wave potential energy is between 2.8% and 13.8%. Shallow initial submergences and lighter specific gravities increase the efficiency with which landslide kinetic energy is converted into wave potential energy. Watts (1997) found conversion rates of solid block kinetic energy into wave potential energy of between 3% and 7%. However, his expression for energy conversion was calculated as a function of the landslide terminal velocity and the square of the maximum wave amplitude. The maximum conversion of landslide potential energy into wave potential energy, presented in Figure 14, range between 1.1% and 5.9%, and are greater for shallower initial submergences. The effect of increasing specific gravity is relatively weaker. Weigel (1955) found typical rates of 1-2% for conversion of landslide potential energy into wave potential energy. His wave potential energies were calculated as a function of the sum of the 1st wave trough and 2nd wave crest amplitudes, squared.

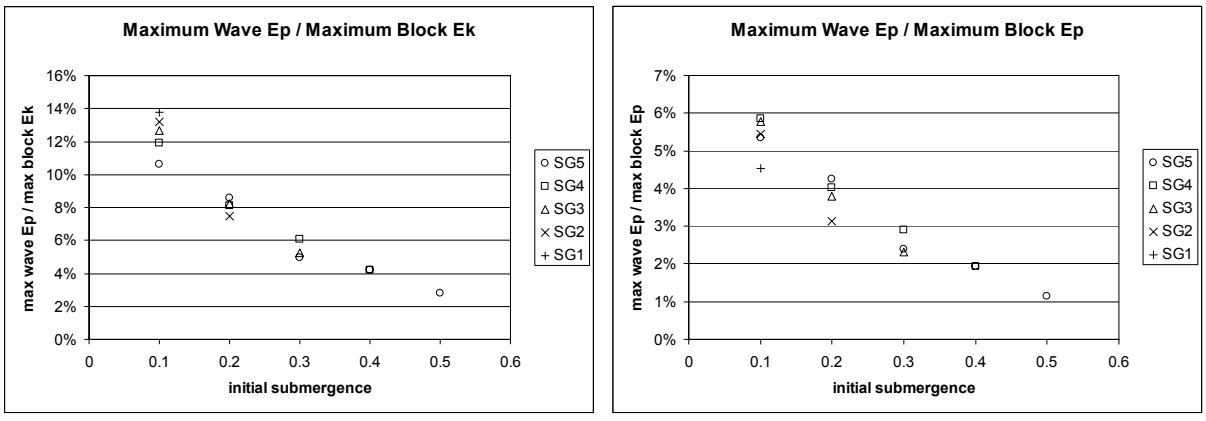


**Figure 14. Percentage conversion of maximum landslide kinetic energy into wave potential energy and maximum landslide potential energy into wave potential energy**

## 4. CONCLUSIONS

The focus of this research was to generate underwater landslide-induced tsunami water level data of sufficient quality for comprehensive verification of numerical model results. The experiments carried out here were for a prismatic semi-elliptical block sliding in water 0.435 m deep, along a 15° slope. Techniques utilising PTV and LIF were used to measure the landslide kinematics and water surface profile time histories for fifteen combinations of landslide specific gravity and initial submergence. Rigorous controls were implemented to ensure the repeatability of these tests. The LIF technique developed to measure the spatial and temporal evolution of the water surface was found to produce results with resolution and accuracy comparable to those of traditional electrical point wave gauges.

The measurement of full water surface profile time histories proved advantageous for closely observing and quantifying the initial generation and propagation of laboratory tsunami waves. By comparing the instantaneous position and speed of the landslide relative to the wave field, it was found that the 1$^{st}$ crest formed over the front half of the landslide and a trough formed over the rear. The point at which these two waves met was centred above the landslide centre of mass and remained there as the block slid down the slope.

Wavelengths of individual waves increased as they propagated due to the waves entering deeper water. The dispersion of the waves was evident, as waves further behind in the wave train propagated more slowly than those in front. New waves were continually generated at the trailing end of the wave train. The wave trough initially generated above the rear end of the landslide propagated in both upstream and downstream directions. The upstream-travelling trough was found to cause the large initial draw-down at the shore. The maximum wave run-up height observed at the shore was found to be caused by a wave crest generated by the landslide as it decelerated at the bottom of the slope.

The ability to resolve water levels spatially and temporally allowed wave potential energy time histories to be calculated. Conversion efficiencies for landslide potential energy into wave potential energy ranged from 1.1%-5.9%. Rates for conversion between landslide kinetic energy and wave potential energy ranged between 2.8% and 13.8%.

## ACKNOWLEDGEMENTS

A substantial portion of this research was made possible with the financial assistance of the New Zealand Earthquake Commission's Research Foundation (reference 6UNI1/506).

## REFERENCES

Davies, H. L., Davies, J. M., Perembo, R. C. B., and Lus, W. Y. (2003). "The Aitape 1998 tsunami: Reconstructing the event from interviews and field mapping." *Pure and Applied Geophysics*, 160(10-11), 1895-1922.

Enet, F., Grilli, S. T., and Watts, P. "Laboratory Experiments for Tsunamis Generated by Underwater Landslides: Comparison with Numerical Modeling." *Proceedings of the Thirteenth (2003) International Offshore and Polar Engineering Conference, May 25 2003-May 30 2003*, Honolulu, HI, United States, 1717-1724.

Fleming, J. G., Walters, R. A., Sue, L. P., and Nokes, R. I. (2005). "Experimental Design For Solid Block and Granular Submarine Landslides: A Unified Approach." Tsunamis: Case Studies and Recent Developments, K. Satake, ed., Springer, 259-277.

Fritz, H. M., Hager, W. H., and Minor, H. E. (2001). "Lituya Bay Case: Rockslide Impact and Wave Run-up." *Science of Tsunami Hazards*, 19(1), 3-22.
Grilli, S. T., Kirby, J. T., Liu, P. L. F., Brandes, H., and Fryer, G. J. (2003). "Workshop on Model Validation and Benchmarking For Tsunami Generation by Submarine Mass Failure - Proposal Submitted to NSF." Honolulu, Hawaii.
Grilli, S. T., Vogelmann, S., and Watts, P. (2002). "Development of a 3D numerical wave tank for modeling tsunami generation by underwater landslides." *Engineering Analysis with Boundary Elements*, 26(4), 301-313.
Grilli, S. T., and Watts, P. (1999). "Modeling of waves generated by a moving submerged body. Applications to underwater landslides." *Engineering Analysis with Boundary Elements*, 23(8), 645-656.
Imamura, F., and Hashi, K. (2003). "Re-examination of the source mechanism of the 1998 Papua New Guinea earthquake and tsunami." *Pure and Applied Geophysics*, 160(10-11), 2071-2086.
Jiang, L., and Leblond, P. H. (1992). "The Coupling of a Submarine Slide and the Surface-Waves Which It Generates." *Journal of Geophysical Research-Oceans*, 97(C8), 12731-12744.
Kanoglu, U. "Nonlinear Evolution and Runup of a Solitary Wave Over a Sloping Beach." *Long Waves Symposium*, AUTh, Thessaloniki, Greece, 281-288.
Kennedy, A. B., Chen, Q., Kirby, J. T., and Dalrymple, R. A. (2000). "Boussinesq modeling of wave transformation, breaking, end runup. I: 1D." *Journal of Waterway Port Coastal and Ocean Engineering-Asce*, 126(1), 39-47.
Liu, P. L. F., Wu, T. R., Raichlen, F., Synolakis, C. E., and Borrero, J. C. (2005). "Runup and rundown generated by three-dimensional sliding masses." *Journal of Fluid Mechanics*, 536, 107-144.
Lynett, P. J., Borrero, J. C., Liu, P. L. F., and Synolakis, C. E. (2003). "Field survey and numerical simulations: A review of the 1998 Papua New Guinea tsunami." *Pure and Applied Geophysics*, 160(10-11), 2119-2146.
Mariotti, C., and Heinrich, P. (1999). "Modeling of submarine landslides of rock and soil." *International Journal for Numerical and Analytical Methods in Geomechanics*, 23(4), 335-354.
Martel, S. J. (2004). "Mechanics of landslide initiation as a shear fracture phenomenon." *Marine Geology*, 203(3-4), 319-339.
Murty, T. S. (2003). "Tsunami wave height dependence on landslide volume." *Pure and Applied Geophysics*, 160(10-11), 2147-2153.
New Scientist. (2004). "Hawaiian Tsunami Left a Gift at the Foot of Kohala Volcano." *New Scientist*, 2464(2464), 14.
Nokes, R. I. (2005a). "FluidStream v6.01: User's Guide." Christchurch, New Zealand, Particle Tracking Velocimetry (PTV).
Nokes, R. I. (2005b). "ImageStream v5.01: System Theory and Design." Christchurch, New Zealand, Image Processing.
Okal, E. A. (2003). "T waves from the 1998 Papua New Guinea earthquake and its aftershocks: Timing the tsunamigenic slump." *Pure and Applied Geophysics*, 160(10-11), 1843-1863.
Raichlen, F., and Synolakis, C. E. "Run-up From Three-Dimensional Sliding Masses." *Long Waves Symposium*, AUTh, Thessaloniki, Greece, 247-256.
Ruff, L. J. (2003). "Some aspects of energy balance and tsunami generation by earthquakes and landslides." *Pure and Applied Geophysics*, 160(10-11), 2155-2176.
Rzadkiewicz, S. A., Mariotti, C., and Heinrich, P. (1997). "Numerical simulation of submarine landslides and their hydraulic effects." *Journal of Waterway Port Coastal and Ocean Engineering-Asce*, 123(4), 149-157.
Satake, K., and Tanioka, Y. (2003). "The July 1998 Papua New Guinea earthquake: Mechanism and quantification of unusual tsunami generation." *Pure and Applied Geophysics*, 160(10-11), 2087-2118.

Sue, L. P. (in preparation). "Modeling of Tsunami Generated By Underwater Landslides," PhD thesis, University of Canterbury, Christchurch, New Zealand.
Sue, L. P., Nokes, R. I., and Walters, R. (2006). "Modeling of Tsunami Generated By Underwater Landslides." *EQC 6UNI1/506*, University of Canterbury, Christchurch, New Zealand.
Synolakis, C. E. (1987). "The Runup of Solitary Waves." *Journal of Fluid Mechanics*, 185, 523-545.
Tappin, D. R., Watts, P., and Matsumoto, T. (2003). "Architecture and Failure Mechanism of the Offshore Slump Responsible for the 1998 Papua New Guinea Tsunami." Submarine mass movements and their consequences : 1st international symposium, J. Locat and J. Mienert, eds., Kluwer Academic Publishers, Boston, 383-389.
Tappin, D. R., Watts, P., McMurtry, G. M., Lafoy, Y., and Matsumoto, T. (2001). "The Sissano, Papua New Guinea tsunami of July 1998 - offshore evidence on the source mechanism." *Marine Geology*, 175(1-4), 1-23.
Tarman, H. I., and Kanoglu, U. "Numerical Simulation of Long Wave Runup on a Sloping Beach." *Long Waves Symposium*, AUTh, Thessaloniki, Greece, 273-279.
Tinti, S., and Bortolucci, E. (2000). "Energy of water waves induced by submarine landslides." *Pure and Applied Geophysics*, 157(3), 281-318.
Walters, R. "Tsunami Runup: Model Development and Testing." *Long Waves Symposium*, AUTh, Thessaloniki, Greece, 289-296.
Watts, P. (1997). "Water Waves Generated by Underwater Landslides," PhD, California Institute of Technology, Pasadena, California.
Watts, P. (1998). "Wavemaker curves for tsunamis generated by underwater landslides." *Journal of Waterway Port Coastal and Ocean Engineering-Asce*, 124(3), 127-137.
Watts, P. (2000). "Tsunami features of solid block underwater landslides." *Journal of Waterway Port Coastal and Ocean Engineering-Asce*, 126(3), 144-152.
Watts, P., and Grilli, S. T. "Underwater Landslide Shape, Motion, Deformation, and Tsunami Generation." *Proceedings of the Thirteenth (2003) International Offshore and Polar Engineering Conference, May 25 2002-May 30 2003*, Honolulu, HI, United States, 1709-1716.
Watts, P., Imamura, F., Bengston, A., and Grilli, S. T. "Benchmark cases for tsunamis generated by underwater landslides." *Proceedings of the Fourth International Symposium Waves 2001, Sep 2-6 2001*, San Francisco, CA, 1505-1514.
Wiegel, R. L. (1955). "Laboratory studies of gravity waves generated by movement of submerged body." *American Geophysical Union -- Transactions*, 36(5), 759-774.